Enceladus' extreme heat flux as revealed by its relaxed craters

Michael T. Bland,[1] Kelsi N. Singer,[1] William B. McKinnon,[1] and Paul M. Schenk[2]

Received 14 June 2012; revised 8 August 2012; accepted 9 August 2012; published 15 September 2012.

[1] Enceladus' cratered terrains contain large numbers of unusually shallow craters consistent with deformation by viscous relaxation of water ice under conditions of elevated heat flow. Here we use high-resolution topography to measure the relaxation fraction of craters on Enceladus far from the active South Pole. We find that many craters are shallower than expected, with craters as small as 2 km in diameter having relaxation fractions in excess of 90%. These measurements are compared with numerical simulations of crater relaxation to constrain the minimum heat flux required to reproduce these observations. We find that Enceladus' nominal cold surface temperature (70 K) and low surface gravity strongly inhibit viscous relaxation. Under such conditions less than 3% relaxation occurs over 2 Ga even for relatively large craters (diameter 24 km) and high, constant heat fluxes (150 mW m^{-2}). Greater viscous relaxation occurs if the effective temperature at the top of the lithosphere is greater than the surface temperature due to insulating regolith and/or plume material. Even for an effective temperature of 120 K, however, heat fluxes in excess of 150 mW m^{-2} are required to produce the degree of relaxation observed. Simulations of viscous relaxation of Enceladus' largest craters suggest that relaxation is best explained by a relatively short-lived period of intense heating that decayed quickly. We show that infilling of craters by plume material cannot explain the extremely shallow craters at equatorial and higher northern latitudes. Thus, like Enceladus' tectonic terrains, the cratered regions of Enceladus have experienced periods of extreme heat flux. **Citation:** Bland, M. T., K. N. Singer, W. B. McKinnon, and P. M. Schenk (2012), Enceladus' extreme heat flux as revealed by its relaxed craters, *Geophys. Res. Lett.*, *39*, L17204, doi:10.1029/2012GL052736.

1. Introduction

[2] Despite its small size, Enceladus is currently one of the most geologically active bodies in the Solar System. Observations of the satellite's South Polar Terrain (SPT) by the Cassini spacecraft have revealed an essentially crater-free (i.e., very young), highly tectonized surface dominated by roughly-parallel fissures dubbed "tiger stripes" [*Porco et al.*, 2006], which are the source of extensive plumes of gas and dust [e.g., *Spitale and Porco*, 2007]. Cassini's Composite Infrared Spectrometer (CIRS) instrument has measured extremely high power emission in the SPT: 15.8 ± 3.1 GW [*Howett et al.*, 2011]. If averaged over the region (e.g., south of 65°S), the emitted power corresponds to heat fluxes of ~400 mW m^{-2}. High resolution CIRS data indicates, however, that the regions of elevated heat flows are strongly associated with the tiger stripes themselves [*Spencer et al.*, 2006; *Howett et al.*, 2011].

[3] In addition to the SPT, two other extensive, quasi-circular regions of Enceladus' surface have been tectonically modified: one centered on the leading hemisphere, and one centered on the trailing hemisphere [e.g., *Porco et al.*, 2006; *Spencer et al.*, 2009; *Crow-Willard and Pappalardo*, 2011]. Together with the SPT, these regions cover a little more than 50% of the satellite [*Crow-Willard and Pappalardo*, 2011]. Numerical modeling of the tectonic surface deformation in these regions suggest that, like the SPT, heat fluxes likely were quite high at the time of disruption: 110-to-270 mW m^{-2} [*Bland et al.*, 2007; *Giese et al.*, 2008], larger than typical terrestrial heat fluxes, and much larger than the roughly 1-to-3 mW m^{-2} expected radiogenic heat flux at Enceladus. The evidence for similar geologic disruption styles in spatially and temporally separated regions has lead to the inference that Enceladus undergoes quasi-episodic periods of localized high heat flow and tectonic disruption [*Helfenstein et al.*, 2006; *O'Neill and Nimmo*, 2010].

[4] Outside of these tectonized regions, Enceladus' surface is dominated by cratered terrains with few tectonic features and age estimates ranging from 1 Ga [*Kirchoff and Schenk*, 2009] to 2 Ga [*Porco et al.*, 2006], assuming the updated cometary cratering fluxes of *Dones et al.* [2009] (age uncertainties are large). The most notable characteristic of the cratered terrain is the large number of impact craters displaying morphologies consistent with viscous relaxation (e.g., shallow depths, up-domed floors) [e.g., *Smith et al.*, 1982; *Passey*, 1983]. These viscously relaxed craters are markers of elevated past heat flow [e.g., *Passey*, 1983], and therefore belie the notion that Enceladus' cratered terrain has been geologically quiescent throughout the satellite's history.

[5] In this paper we utilize high-resolution topography data produced by stereo-controlled photoclinometry to characterize the degree of relaxation (i.e., their current apparent depth relative to their expected initial depth) for a sub-set of craters on Enceladus. These observations are compared to finite element simulations of the viscoelastic relaxation of impact craters to place quantitative constraints on the long-term heat flux in Enceladus' cratered terrains. We find that, even when using conservative assumptions (i.e., assumptions that enhance relaxation), heat fluxes in the cratered terrain must have been >150 mW m^{-2}. We suggest then, that even Enceladus' endogenically inactive regions have had a spectacular (and possibly non-uniform) thermal history.

2. Measuring Crater Relaxation on Enceladus

[6] We measured apparent crater depths (i.e., crater depth relative to the surrounding ground plain) using ArcGIS in two regions on Enceladus (Figure 1). Within these two regions

[1]Department of Earth and Planetary Sciences and McDonnell Center for the Space Sciences, Washington University, Saint Louis, Missouri, USA.
[2]Lunar and Planetary Institute, Houston, Texas, USA.

Corresponding author: M. T. Bland, Department of Earth and Planetary Sciences, Washington University, Campus Box 1169, 1 Brookings Dr., Saint Louis, MO 63130, USA. (mbland@levee.wustl.edu)

©2012. American Geophysical Union. All Rights Reserved.
0094-8276/12/2012GL052736

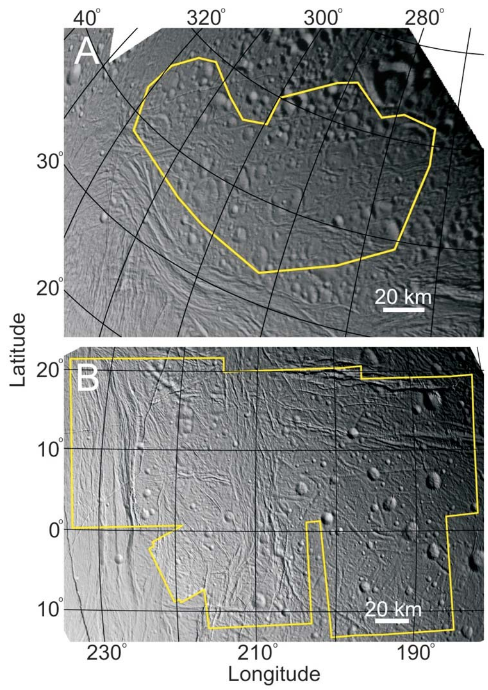

Figure 1. The two regions in which crater relaxation was measured (outlined in yellow) (a) north of Hamah Sulci (24 craters) and (b) east of Harran Sulci (127 craters). See Figure S1 for context map.

data were acquired for 151 craters for which the illumination geometry provided robust topography (127 equatorial craters, 24 craters north of Hamah Sulcus). Crater topography was derived from high resolution Cassini ISS images using stereo-controlled photoclinometry. The technique has been described in detail elsewhere [see, e.g., *Schenk*, 2002; *Bray et al.*, 2012]. The combined stereo/photoclinometry technique provides a robust topographic data set at both long and short wavelengths with vertical precisions of a few 10s of meters. Details of the measurement techniques and the uncertainties are provided in the auxiliary material.[1]

[7] From the apparent crater depths (d_a), the degree of relaxation (i.e., the relaxation fraction (*RF*)) can be calculated if an initial apparent crater depth ($d_{a,i}$) is assumed ($RF = 1 - d_a/d_{a,i}$). Initial crater depths are derived from lunar depth-diameter relations, which are applicable to simple craters on the terrestrial planets [e.g., *Melosh*, 1989] and the icy Galilean satellites [*Schenk*, 2002] (see auxiliary material). The relaxation fraction for all 151 craters plotted against their crater diameter is shown in Figure 2. In general, craters on Enceladus are highly relaxed. All measured craters over ~12 km were effectively completely relaxed (i.e., only short-wavelength topography remains). Smaller craters (<10 km) show greater variability in their relaxation state. Even some of the smallest craters measured (~2 km diameter) have undergone more than 90% relaxation: a notable observation considering the difficulty involved in relaxing short-wavelength topography [e.g., *Scott*, 1967; *Parmentier and Head*, 1981]. That relaxed craters exist on Enceladus has been known since Voyager 2 [*Smith et al.*, 1982; *Passey*, 1983]; however, our measurements emphasize the extreme degree of viscous relaxation that has occurred at even small crater sizes, unresolvable in Voyager imagery.

3. Modeling Crater Relaxation

[8] In order to constrain the thermal conditions required to produce the degree of viscous relaxation observed on Enceladus we simulate crater relaxation in axisymmetric geometry using the viscoelastic finite element code Tekton [*Melosh and Raefsky*, 1980]. The code has been modified and used extensively to model the tectonic deformation of ice lithospheres [e.g., *Bland et al.*, 2007]. Simulations were performed following the approach of *Dombard and McKinnon* [2006], and a more detailed description of our methodology is available there and in the auxiliary material.

[9] We simulate the viscous relaxation of craters with diameters between 4 and 34 km over timescales up to 2 Ga, consistent with the maximum estimated surface age of the cratered terrains. Because fresh craters are uncommon on Enceladus [*Kirchoff and Schenk*, 2009] (Figure 2), and to allow greater consistency between simulated craters, we utilized standardized, simple, parabolic initial crater shapes with initial rim-to-floor depths given by $d/D = 0.2$ (where d is the rim-to-floor depth and D is the rim-to-rim diameter), rim heights of $h_{rim} = 0.036D$, and rim topography (ejecta plus

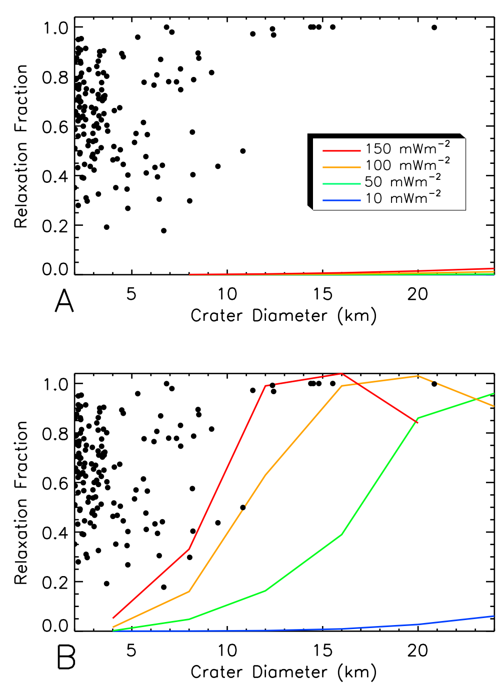

Figure 2. Relaxation fraction as a function of crater diameter for measured Enceladus craters (black dots, n = 151) and simulated craters at four different values of constant heat flux (curves) after 2 Ga using (a) Enceladus' nominal average blackbody surface temperature of 70 K and (b) a lithospheric surface temperature of 120 K. Relaxation fraction in the numerical simulations is measured analogously to Enceladus' actual craters: the average depth of the crater center (within one-third crater radius)is averaged with the deepest point; see auxiliary material for details.

[1]Auxiliary materials are available in the HTML. doi:10.1029/2012GL052736.

uplift) that falls off as $1/r^3$ (i.e., we follow fresh, lunar simple crater geometry [*Pike*, 1977]).

[10] We investigate heat fluxes between 10 and 150 mW m^{-2}. Tekton does not include thermodynamics (i.e, temperature, heat flow, viscous dissipation are not solved for), but viscosity structures that correspond to pre-defined heat fluxes can be modeled. Enceladus' nominal surface temperature is 70 K; however, *Passey and Shoemaker* [1982] and *Passey* [1983] argued that the temperature at the top of Enceladus' ice *lithosphere* may exceed the surface temperature if it is overlain by a strongly insolating regolith. Measurements of the thermal conductivity of fine-grained, powdered water-ice samples in vacuum indicate values several orders of magnitude lower than intact ice [*Seiferlin et al.*, 1996; *Ross and Kargel*, 1998], suggesting that a few meters of regolith (or plume material) can strongly modulate the temperature at the top of Enceladus' lithosphere [see also *Nimmo et al.*, 2003, Appendix B]. The temperature at the base of an ice regolith is self limiting due to annealing of ice grains [*Passey and Shoemaker*, 1982; *Nimmo et al.*, 2003]; we therefore investigate relaxation for range of individual surface temperatures between 70 K and 120 K (near the suggested effective surface temperature of *Passey and Shoemaker* [1982]).

[11] We model Enceladus' lithosphere with a viscoelastic rheology appropriate for ice Ih. We assume the ice lithosphere is solid and coherent with a Young's modulus of 9.3 GPa, and a Poisson's ratio of 0.325 [*Gammon et al.*, 1983]. We incorporate viscous deformation with a composite flow law that includes dislocation creep, grain boundary sliding (GBS), basal slip (BS), and diffusion creep. The GBS and diffusion creep flow mechanisms are grain size dependent. We use a nominal grain size of 1 mm, consistent with grain sizes in terrestrial glaciers [e.g., *De La Chappelle et al.*, 1998], and theoretical estimates from icy satellite convection models [*Barr and McKinnon*, 2007] (see below). At the maximum stresses typical of our simulations ($\sim 10^4$–10^5 Pa), for larger craters grain-size-sensitive creep mechanisms dominate viscous deformation [see *Durham and Stern*, 2001].

4. Model Results

[12] Figure 2 shows curves of relaxation fraction as a function of crater diameter for four constant heat fluxes applied over 2 Ga. Figure 2a demonstrates that Enceladus' nominal cold surface temperature (70 K) and low gravitational acceleration strongly inhibit viscous relaxation. Even under high heat fluxes (150 mW m^{-2}), relatively large craters (24 km diameter) relax by less than 3% over 2 Ga. Small craters (<10 km) undergo negligible relaxation even at the highest heat fluxes investigated.

[13] The absence of viscous relaxation under Enceladus-like conditions in our simulations is consistent with *Passey* [1983], who found from analytical models of Newtonian relaxation that Enceladus' nominal lithosphere was too viscous to allow relaxation of crater topography. Following the suggestion of *Passey* [1983], we have investigated viscous relaxation of impact craters using a warmer surface temperature boundary condition (as described above). Alternatively, Enceladus' lithosphere could contain some component (e.g., ammonia) that decreases its viscosity below that of pure water ice; however because low-stress, grain-size-sensitive rheologies of ammonia-water ices have not been measured [*Durham et al.*, 1993], we currently only examine the role of lithospheric surface temperature.

[14] Figure 2b is identical to Figure 2a but uses a lithospheric surface temperature of 120 K. As expected, with a higher surface temperature (and therefore greater temperatures at depth for a given heat flow), viscous relaxation occurs more readily. For craters larger than ~16 km in diameter, significant relaxation (≥40%) occurs when constant heat fluxes of 50 mW m^{-2} or more are applied over 2 Ga. These craters show the up-domed floors characteristic of viscously relaxed craters. At very high heat flows relaxation fractions appear to decrease modestly as crater size increases. This is due to the averaging technique used to calculate the crater depth, and hence the relaxation fraction as well (as described in the figure caption). At crater sizes below 10 km, some relaxation (10–30%) occurs when the highest heat fluxes in our study are applied (150 mW m^{-2}). Yet even with a lithospheric surface temperature 50 K above Enceladus' nominal average surface temperature and heat fluxes that exceed the expected radiogenic heating (average of ~1 mW m^{-2} over the last 2 Ga) by two orders of magnitude, our simulations cannot produce the degree of relaxation actually observed for small craters.

[15] We have so far assumed constant heat fluxes sustained over long periods of time, the fluxes above should be regarded as underestimates of peak values. In reality, a shorter-lived, higher-amplitude heat pulse may be more geologically plausible than the sustained heat fluxes examined. Evidence for such a scenario comes from Enceladus' morphologically distinctive "central mound" craters Aladdin and Ali Baba. These craters, located outside the two study regions described above, have large central structures that extend to roughly half the crater radius and tower to nearly 1 km above the surrounding terrain (Figure 3).

[16] Comparison between topographic profiles across the central mound crater Aladdin, and topography profiles produced by our viscous relaxation simulations of similarly sized craters (Figure 3) suggest that the basic shape of the central mound craters can be reproduced by viscous relaxation under high heat fluxes for short periods of time (e.g., 150 mW m^{-2} over 2 Ma, with T_s = 120 K for the simulated crater in Figure 3). Both simulated and real topography profiles exhibit uplifted rims, deep circumferential troughs inside the crater rim, and broad central structures that rise to ~1 km above the surrounding terrain. The central mound morphology shown in Figure 3 is best matched by an initial crater with a modest central peak, which is plausible given the simple-to-complex morphological transition at a diameter of ~25 km observed on Mimas [*Kirchoff and Schenk*, 2009, Figure 9].

[17] The central mound morphology is a result of the wavelength dependence of viscous relaxation: long topographic wavelengths (i.e., the crater bowl) relax quickly, lifting the shorter-wavelength (and slowly relaxing) central peak well above the surrounding plain. The morphology shown in Figure 3 is transient. As relaxation continues the uplifted crater floor subsides, leaving only relatively subdued, shorter-wavelength topography. Preserving a large central mound therefore requires that the heating event that causes relaxation end before the crater completely relaxes. Assuming T_s = 120 K, heat fluxes of 50–100 mW m^{-2} reproduce the morphology, but require the heating to end by ~20 Ma and ~3 Ma, respectively, to prevent the crater from becoming over-relaxed. Heat fluxes below 50 mW m^{-2} fail

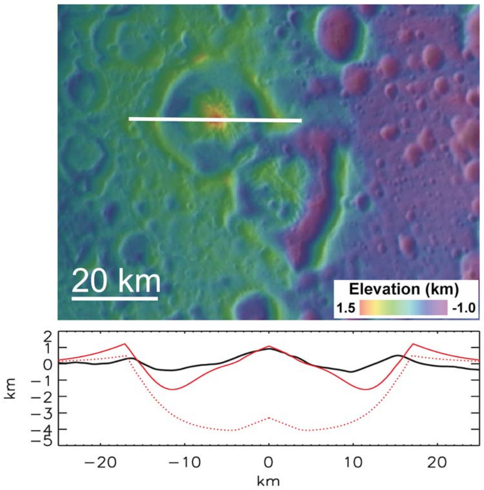

Figure 3. (top) Stereo-controlled photoclinometry data overlaid on Cassini ISS image of two central mound craters (Aladdin and Ali Baba; see Figure S1 for locations). The horizontal white bar marks the position of the topography profile shown below. (bottom) Topography profile across the crater Aladdin (black line). Also shown is the initial (red dotted line) and final (red solid line) shape of a simulated relaxed crater with D = 34 km after 2 Ma under a heat flux of 150 mW m^{-2}. The initial crater shape is a 4th order polynomial with d_a/D consistent with lunar complex craters from *Pike* [1977], but with a simple-to-complex transition diameter of 25 km.

to reproduce the morphology due to insufficient uplift of the crater center. Decreasing the lithospheric surface temperature requires an increase in the heat flux; however, very cold surface temperatures (e.g., T_s = 70 K) prevent sufficient crater relaxation at any heat flux in the range investigated by us. If central mound craters are produced by viscous relaxation, their presence suggests not only warm lithospheric surface temperatures but also transient pulses of extremely high heat fluxes, rather than sustained, lower heat fluxes.

5. Discussion

5.1. Can Plume Fallout Erase Craters on Enceladus?

[18] Crater counts on Enceladus by *Kirchoff and Schenk* [2009] indicate that Enceladus is deficient in impact craters greater than 6 km in diameter relative to the other Saturnian satellites. This dearth of impact craters has been attributed to a combination of viscous relaxation and burial by plume or E-ring material [*Kirchoff and Schenk*, 2009]. Our modeling indicates that viscous relaxation alone probably cannot completely remove (i.e., "erase") the topography of even Enceladus' larger (20 km diameter) impact craters, for "reasonable" heat flows. From these simulations, however, we can place bounds on the volume of plume material required to completely bury the remaining post-relaxation crater.

[19] A 20-km-diameter crater, submitted to a constant heat flux of 150 mW m^{-2} for 1 Ga with a lithospheric surface temperature of 120 K will relax by ∼87% as measured from the average floor depth (Figure 2) or ∼82% as measured to the deepest point in the crater. Assuming an initial true crater depth of 4 km (i.e., rim-to-floor depth given by d/D = 0.2) and a rim height one-fifth the total depth, a crater with an average and maximum apparent depth of 420 m and 580 m will remain. Current *maximum* deposition rates in the equatorial region are ∼10^{-3} mm yr^{-1} (decreasing to the north and away from the 45°/225°W longitude band) [*Kempf et al.*, 2010], requiring at least ∼500 Ma of sustained deposition to fill the crater. If the deposition rate was lower (say, ∼10^{-4} mm yr^{-1}), or active only episodically (say, 10% of the time), the time scale for crater erasure exceeds the age of the Solar System. For smaller craters, the degree of viscous relaxation resulting from a sustained heat flux is substantially less, but their shallower depth requires less material to fill. Under the conditions described above, an 8 km-diameter crater with an initial apparent depth of 1.28 km relaxes by a maximum of 22% leaving a crater nearly 1 km deep. As in the case of the 20 km crater, infilling by plume material could plausibly erase such a crater over a billion year timescales, but only assuming high, and sustained, deposition rates. Notably, deposition of plume material is negligible in our mid-latitude study area north of Hamah Sulcus [*Kempf et al.*, 2010].

[20] Fundamentally, the complete removal of craters by relaxation and plume burial alone is problematic under the conditions investigated here because too little viscous relaxation occurs under even large, sustained heat fluxes. If small to mid-sized craters have been removed from the surface, heat fluxes must have been well in excess of 150 mW m^{-2} or the rate of material deposition must have been substantially higher. The latter may require that the locus of plume activity has shifted throughout Enceladus' history [e.g., *Helfenstein et al.*, 2006; *Spencer et al.*, 2009], permitting significantly higher deposition rates of plume material near the cratered terrains (e.g., deposition rates within the SPT can exceed ∼10^{-2} mm yr^{-1}). Impact erosion and regolith formation also act to reduce crater topography, but not in a way that mimics relaxation. Alternatively, very small ice grain sizes (∼100 μm), brittle failure viscosity-reducing ice contaminants, or even warmer effective surface temperatures could all promote greater viscous relaxation; however, the plausibility of the first of these is questionable, and substantially relaxing small craters will remain challenging without high heat flow (see auxiliary material).

5.2. Enceladus' Thermal History

[21] The high heat fluxes inferred for Enceladus' heavily cratered terrain alters common conceptions of the satellite's geologic history. Several authors have posited the idea that Enceladus has experienced episodic periods of spatially localized high heat fluxes and tectonic disruption. Whereas such localized tectonic disruptions clearly have occurred, the results presented here indicate that (1) periods of high heat flux have occurred on Enceladus without being accompanied by faulting, folding or similar tectonic deformation, and/or (2) that regions of high heat fluxes were not particularly localized.

[22] Constraining the relative timing of the heating event(s) that caused viscously relaxation of Enceladus' craters is difficult. Since most mid-sized (10-to-30 km diameter) craters are at least partially relaxed, however, the high heat fluxes must have persisted into geologically recent times (or else numerous mid-sized unrelaxed craters should be observed). While the cratered terrains are significantly older than Enceladus' tectonic terrains, the viscous relaxation event(s) plausibly could have occurred during the same epoch of high heat fluxes that led to the formation of the equatorial tectonic

regions, which lie in close proximity to the cratered terrains. Crater counts suggest that these tectonic regions have variable ages from 10 to 170 Ma [*Porco et al.*, 2006; *Kirchoff and Schenk*, 2009]. Thus, these tectonic regions could have formed concurrently with viscous relaxation in cratered terrains, with spatial variations in heat fluxes or local stress fields producing tectonic disruption in some areas, but only viscous relaxation in others. Whatever the scenario, we emphasize that the heat fluxes that have been inferred here for Enceladus' cratered terrain (150 mW m^{-2}) are consistent with heat fluxes inferred for its tectonic regions (110–270 mW m^{-2} [*Bland et al.*, 2007; *Giese et al.*, 2008]), and are of the same order (though lower by a factor of 2 or 3) as the measured values spatially averaged over the SPT. Clearly, the entire satellite has experienced a spectacular, and highly variable thermal history.

[23] **Acknowledgments.** This work was supported by NASA's Cassini Data Analysis Program grant NNX11AK76G, and by a NESS fellowship to K.N.S.

[24] The Editor thanks John Spencer and William B. Durham for their assistance in evaluating this paper.

References

Barr, A. C., and W. B. McKinnon (2007), Convection in ice I shells and mantles with self-consistent grain size, *J. Geophys. Res.*, *112*, E02012, doi:10.1029/2006JE002781.

Bland, M. T., R. A. Beyer, and A. P. Showman (2007), Unstable extension of Enceladus' lithosphere, *Icarus*, *192*, 92–105, doi:10.1016/j.icarus.2007.06.011.

Bray, V. J., P. M. Schenk, H. J. Melosh, J. V. Morgan, and G. S. Collins (2012), Ganymede crater dimensions: Implications for central peak and central pit formation and development, *Icarus*, *217*, 115–129, doi:10.1016/j.icarus.2011.10.004.

Crow-Willard, E., and R. T. Pappalardo (2011), Global geological mapping of Enceladus, EPSC-DPS Joint Meeting, Eur. Planet. Sci. Congr., Nantes, France.

De La Chappelle, S., O. Castelnau, V. Lipenkov, and P. Duval (1998), Dynamic recrystalization and tecture development in ice as revealed by the study of deep ice cores in Antartica and Greenland, *J. Geophys. Res.*, *103*, 5091–5105.

Dombard, A. J., and W. B. McKinnon (2006), Elastoviscoplastic relaxation of impact crater topography with application to Ganymede and Callisto, *J. Geophys. Res.*, *111*, E01001, doi:10.1029/2005JE002445.

Dones, L., C. R. Chapman, W. B. McKinnon, H. J. Melosh, M. R. Kirchoff, G. Neukum, and K. J. Zahnle (2009), Icy satellites of Saturn: Impact cratering and age determination, in *Saturn from Cassini-Huygens*, edited by M. K. Dogherty, L. W. Esposito, and S. M. Krimigis, pp. 613–635, Springer, Dordrecht, Netherlands.

Durham, W. B., and L. A. Stern (2001), Rheological properties of water ice: Applications to satellites of the outer solar system, *Annu. Rev. Earth Planet. Sci.*, *29*, 295–330.

Durham, W. B., S. H. Kirby, and L. A. Stern (1993), Flows of ices in the ammonia-water system, *J. Geophys. Res.*, *98*, 17,667–17,682.

Gammon, P. H., H. Klefte, and M. J. Clouter (1983), Elastic constants of ice samples by Brillouin spectroscopy, *J. Phys. Chem.*, *87*, 4025–4029.

Giese, B., R. Wagner, H. Hussmann, G. Neukum, J. Perry, P. Helfenstein, and P. C. Thomas (2008), Enceladus: An estimate of heat flux and lithospheric thickness from flexurally supported topography, *Geophys. Res. Lett.*, *35*, L24204, doi:10.1029/2008GL036149.

Helfenstein, P., et al. (2006), Surface geology and tectonism on Enceladus, *Eos Trans. AGU*, *87*(52), Fall Meet. Suppl., Abstract P22B-02.

Howett, C. J. A., J. R. Spencer, J. Pearl, and M. Segura (2011), High heat flow from Enceladus' south polar region measured using 10–600 cm^{-1} Cassini/CIRS data, *J. Geophys. Res.*, *116*, E03003, doi:10.1029/2010JE003718.

Kempf, S., U. Beckmann, and J. Schmidt (2010), How the Enceladus dust plume feeds Saturn's E ring, *Icarus*, *206*, 446–457, doi:10.1016/j.icarus.2009.09.016.

Kirchoff, M. R., and P. Schenk (2009), Crater modification and geologic activity in Enceladus' heavily cratered plains: Evidence from the impact crater distribution, *Icarus*, *202*, 656–668, doi:10.1016/j.icarus.2009.03.034.

Melosh, H. J. (1989), *Impact Cratering: A Geologic Process*, Oxford Univ. Press, New York.

Melosh, H. J., and A. Raefsky (1980), The dynamical origin of subduction zone topography, *Geophys. J. R. Astron. Soc.*, *60*, 333–354.

Nimmo, F., R. T. Pappalardo, and B. Giese (2003), On the origins of band topography, Europa, *Icarus*, *166*, 21–32.

O'Neill, C., and F. Nimmo (2010), The role of episodic overturn in generating the surface geology and heat flow on Enceladus, *Nat. Geosci.*, *3*, 88–91, doi:10.1038/ngeo731.

Parmentier, E. M., and J. W. Head (1981), Viscous relaxation of impact craters on icy satellite surfaces: Determination of viscosity variation with depth, *Icarus*, *47*, 100–111.

Passey, Q. R. (1983), Viscosity of the lithosphere of Enceladus, *Icarus*, *53*, 105–120.

Passey, Q. R., and E. M. Shoemaker (1982), Craters and basins on Ganymede and Callisto: Morphological indicators of crustal evolution, in *Satellites of Jupiter*, edited by D. Morrison, pp. 379–434, Univ. of Ariz. Press, Tucson.

Pike, R. (1977), Size-dependence in the shape of fresh impact craters on the Moon, in *Impact and Explosion Cratering*, edited by D. J. Roddy, R. O. Pepin, and R. B. Merrill, pp. 489–509, Pergamon, New York.

Porco, C. C., et al. (2006), Cassini observes the active south pole of Enceladus, *Science*, *311*, 1393–1401.

Ross, R. G., and J. S. Kargel (1998), Thermal conductivity of solar system ices with special reference to the Martian polar caps, in *Solar System Ices*, edited by B. Schmitt, C. de Bergh, and M. Feslov, pp. 33–62, Kluwer Acad., Dordrecht, Netherlands.

Schenk, P. M. (2002), Thickness constraints on the icy shells of the Galilean satellites from a comparison of crater shapes, *Nature*, *417*, 419–421.

Scott, R. F. (1967), Viscous flow of craters, *Icarus*, *7*, 139–148.

Seiferlin, K., N. I. Kömle, G. Kargl, and T. Spohn (1996), Line heat-source measurements of the thermal conductivity of porous H_2O ice, CO_2 ice and mineral powders under space conditions, *Planet. Space Sci.*, *44*, 691–704, doi:10.1016/0032-0633(96)00068-2.

Smith, B. A., et al. (1982), A new look at the Saturn system: The Voyager 2 images, *Science*, *215*, 504–537.

Spencer, J. R., et al. (2006), Cassini encounters Enceladus: Background and the discovery of a south polar hot spot, *Science*, *311*, 1401–1405.

Spencer, J. R., et al. (2009), Enceladus: An active cryovolcanic satellite, in *Saturn From Cassini-Huygens*, edited by M. K. Dougherty, L. W. Esposito, and S. M. Krimigis, pp. 683–724, Springer, Dordrecht, Netherlands.

Spitale, J. N., and C. C. Porco (2007), Association of the jets of Enceladus with the warmest regions on its south-polar fractures, *Nature*, *449*, 695–697, doi:10.1038/nature06217.